ResearchGate

See discussions, stats, and author profiles for this publication at: https://www.researchgate.net/publication/270397783

Compaction of porous ices rich in water by swift heavy ions

ARTICLE *in* ICARUS · APRIL 2015

Impact Factor: 3.04 · DOI: 10.1016/j.icarus.2014.12.002

CITATIONS
4

READS
21

8 AUTHORS, INCLUDING:

A. L. F. de Barros
Centro Federal de Educação Tecnológica C…
44 PUBLICATIONS **255** CITATIONS
SEE PROFILE

Emerson Duarte
Federal University of Pará
70 PUBLICATIONS **2,074** CITATIONS
SEE PROFILE

Enio Frota da Silveira
Pontifícia Universidade Católica do Rio de …
179 PUBLICATIONS **1,173** CITATIONS
SEE PROFILE

Alicja Domaracka
Centre de Recherche sur les Ions, les Matéri…
112 PUBLICATIONS **633** CITATIONS
SEE PROFILE

All in-text references underlined in blue are linked to publications on ResearchGate, letting you access and read them immediately.

Available from: Christian F. Mejía G.
Retrieved on: 27 January 2016

Icarus 250 (2015) 222–229

Contents lists available at ScienceDirect

Icarus

journal homepage: www.elsevier.com/locate/icarus

Compaction of porous ices rich in water by swift heavy ions

C. Mejía [a,*], A.L.F. de Barros [b], E. Seperuelo Duarte [c], E.F. da Silveira [a], E. Dartois [d,e], A. Domaracka [f], H. Rothard [f], P. Boduch [f]

[a] Departamento de Física, Pontifícia Universidade Católica do Rio de Janeiro, Rua Marquês de São Vicente 225, 22451-900 Rio de Janeiro, RJ, Brazil
[b] Departamento de Física, Centro Federal de Educação Tecnológica Celso Suckow da Fonseca, Av. Maracanã 229, 20271-110 Rio de Janeiro, RJ, Brazil
[c] Grupo de Física e Astronomia, Instituto Federal de Educação Ciência e Tecnologia do Rio de Janeiro, Rua Lúcio Tavares, 1045, 2653-060 Nilópolis, RJ, Brazil
[d] CNRS-INSU, Institut d'Astrophysique Spatiale, UMR 8617, 91405 Orsay, France
[e] Université Paris Sud, Institut d'Astrophysique Spatiale, UMR 8617, bâtiment 121, 91405 Orsay, France
[f] Centre de Recherche sur les Ions, les Matériaux et la Photonique (CEA/CNRS/ENSICAEN/Université de Caen-Basse Normandie), CIMAP-CIRIL-Ganil, Boulevard Henri Becquerel, BP 5133, F-14070 Caen Cedex 05, France

ARTICLE INFO

Article history:
Received 15 July 2014
Revised 28 November 2014
Accepted 1 December 2014
Available online 10 December 2014

Keyword:
Cosmic rays
Solar wind ices
IR spectroscopy collisional physics

ABSTRACT

Porous water ice and water ice mixtures H_2O:X (X = CO, CO_2 and CH_4) produced at 15 K, with film thicknesses in the 0.5–1 μm range, were irradiated by swift ions and monitored by mid-infrared spectroscopy (FTIR). The analysis of the evolution of the pure water ice infrared absorption on ion beam dose reveals a strong correlation among three quantities: (i) the absorbance of the most intense band (3250 cm^{-1}), (ii) the wavelength of the maximum absorbance of this band and (iii) the absorbance of the OH-dangling bonds. This correlation is interpreted as indications of the water ice compaction by irradiation: as the beam fluence increases, the ice porosity decreases, the dangling bond peaks collapse and the area and position of the 3250 cm^{-1} band vary exponentially, all of them evolving with the same compaction cross section (σ_c). The linear dependence $\sigma_c \propto S_e$ (S_e being the electronic stopping power) is observed for both pure and mixed water ices, confirming previous results. We suggests that the infrared absorption *A*-value varies with dose as $(1-\zeta e^{-D/D_0})$ during the compaction process ($D_0 = 0.2$ eV/molec being the effective energy density to eliminate the OH-db, and ζ is a parameter characterizing the porosity). These findings may be used as a diagnostic tool to probe the morphology of water ices occurring in the outer Solar System and in the ISM.

© 2014 Elsevier Inc. All rights reserved.

1. Introduction

Water vapor was detected for the first time by Cheung et al. (1969) in the Orion nebula, Sgr B2 and W49, via observation of microwave radiation from water molecule rotational transition. Infrared spectroscopy has shown the presence of water ice in protostars (Gillett and Forrest, 1973) and in dense interstellar clouds (Whittet, 2003). Observations of water in gas and solid phases were also reported by Gibb et al. (2004), Pontoppidan et al. (2004), Dartois (2005). In the Solar System, water ice is an abundant constituent of the surfaces of some planets or satellites (Smith et al., 1989) of the trans-Neptunian objects (TNO) and of some planetary rings (e.g., those of Saturn). Besides, water is commonly observed in the coma of comets being the most abundant volatile molecule (Mumma and Charnley, 2011).

The physical, chemical and morphological changes of water ice have been extensively studied using charged particle and photon irradiation at different temperatures (e.g. Baragiola, 2003; Collado et al., 2004; de Barros et al., 2011; Johnson, 2011; Yabushita et al., 2013; Baragiola et al., 2013 and references therein). Surface chemical reactions producing morphological changes have been investigated by Oba et al. (2009) and Accolla et al. (2013). The collapse of porous in water ice induced by thermal processes have been analyzed recently by Bossa et al. (2012). To study some of the effects induced by radiation, laboratory experiments have been carried out under physical conditions as close as possible to the astrophysical ones, e.g. (Brown et al., 1978; Lanzerotti et al., 1978; Strazzulla and Palumbo, 1998; Moore and Hudson, 2000; Leto and Baratta, 2003; Ponciano et al., 2005). Fast ions passing through the solid transfer energy to the target material. For projectile velocities around or greater than Bohr velocities ($v_B \sim 0.22$ cm/ns), the electronic stopping power, S_e, is the most important contribution. Atomic cascades and electronic excitations occur, as a consequence, many molecular bonds are broken along the ion track, generating rearrangement of the lattice structure and allowing molecular fragments to recombine into new chemical species (Baragiola et al., 2008; Johnson, 2011).

* Corresponding author.
E-mail address: cfmejiag@gmail.com (C. Mejía).

http://dx.doi.org/10.1016/j.icarus.2014.12.002
0019-1035/© 2014 Elsevier Inc. All rights reserved.

One of the first phenomena produced by irradiation of initially crystalline water ice is amorphization (Leto and Baratta, 2003; Baragiola, 2003); this morphological state is expected to occur extensively in the astrophysical ices. The water morphological changes have been largely studied using different techniques and irradiation sources. Parent et al. (2002) studied the structure of p-ASW (porous amorphous solid water) using near-edge X-ray absorption fine structure to determine the size and distribution of pores. Leto and Baratta (2003) irradiated porous and crystalline water ice with photons (10.2 eV) and with ions (30 keV H^+ and 60 keV Ar^{++}). Baratta et al. (2004) showed that the compaction produced after ions irradiation of p-ASW is correlated with the decrease of OH dangling bonds (OH-db). Raut et al. (2008) measured the porosity of p-ASW during ion irradiation and calculated the density of the ice film from the reduction of the ice thickness. In a previous paper, Raut et al. (2007) have shown that the internal surface area of the pores decreases faster than the volume of the pores; this morphology change was seen in the fast reduction of the OH-db band area. Raut et al. (2007) also found that the non observation of OH-db mode peaks in infrared (IR) spectra does not imply the absence of pores, because observation of tiny OH-db signals in reduced porosity films after irradiation is difficult. Dartois et al. (2013) analyzed the compaction of ice via the evolution of OH-db features by using light and swift heavy ions generated by high doses of irradiation. Such experiments simulate the cosmic ray interaction with ices, causing a synergetic relationship with the OH-db reduction.

The present work describes and discusses the morphological changes of the irradiated water (p-ASW) using data obtained by infrared spectroscopy. The current results demonstrate that spectroscopic changes observed in the band 3250 cm^{-1} are directly connected with the OH-db collapse when irradiated. In addition, the effects due to mixtures of several molecular species with H_2O are studied. The analysis demonstrates that (i) the compaction process can be associated with the OH-stretch mode peak position of the water band (around 3250 cm^{-1}), and (ii) after 10^{12} ions/cm^2 the OH-db feature collapses and a compacted structure is formed.

2. Experimental

The experimental setup was described by Seperuelo Duarte et al. (2009). A high vacuum chamber ($\sim 10^{-7}$ mbar) has in its center a rotatory platform holding a CsI substrate coupled to a closed-cycle helium cryostat. The water vapor was condensed onto the CsI substrate at 15 K during a few minutes until an $\sim$1 μm thick film was formed. The substrate can be rotated into three positions: one for deposition, the second one for irradiation, and another for FTIR spectroscopy. The ice was irradiated by heavy ion beams (40 and 52 MeV Ni with flux around 10^9 ions/cm^2 s, as listed in Table 1) at the GANIL facility in Caen, France. IR absorption spectra were recorded at different fluences; each spectrum covers the 600–5000 cm^{-1} wavenumber range and was acquired through 252 scans with 1 cm^{-1} resolution.

The H_2O:X mixture gases (X = CO, CO_2 and CH_4) were prepared in a dedicated chamber where the desired composition was obtained by setting partial pressures for each gas. Table 1 lists the mixture concentrations, the film thicknesses, the projectile species and their energies, as well as the corresponding electronic stopping power.

3. Laboratory results

The shapes of the infrared absorption features of water ice clearly depend on its structure (Leto and Baratta, 2003). Fig. 1 shows the evolution of the 3250 cm^{-1} band (the most intense one in the mid-IR spectrum) for ice obtained by depositing H_2O vapor at 15 K and irradiating by 46 MeV Ni at several fluences (Dartois et al., 2013). The inset presents the evolution of the two dangling bond peaks which are observed in ices formed by deposition at temperatures lower than about 120 K (Rowland and Paul Devlin, 1991).

Because of surface irregularities or pore asymmetries, small OH dangling bonds at 3720 and 3692 cm^{-1} arise due to unsaturated molecular bonds, these features can vary with temperature or irradiation (Rowland and Paul Devlin, 1991; Palumbo et al., 2010). In general, the OH-stretch mode peak shape changes during ion bombardment: Leto and Baratta (2003) reported that the 3250 cm^{-1} band area increases and its position shifts. The current analysis reveals a direct correlation between these changes observed in the OH-stretch mode and the OH-db band area; additionally, the same behavior in water ice mixtures H_2O:X is observed.

3.1. Band area increase: phenomenological description

Fig. 2a displays the evolution of the 3250 cm^{-1} band area when a p-ASW is irradiated by 46 MeV Ni and by 606 MeV Zn ions. Before irradiation, the measured area of a given peak of a virgin *porous* ice is defined as S_p. Once the irradiation starts, the band area increases (or decreases) rapidly; after a certain fluence, it decreases slow and exponentially with the decay parameter σ_d^{ap}. Extrapolating the exponential behavior seen at large fluences to $F = 0$, one obtains the band area S_0 which should correspond to a virgin *compacted* ice. Therefore, the difference $(S_0 - S_p)$ is caused by the ice porosity and tends to disappear when the sample is irradiated. The dependence of the band area, $S(F)$, on the ion beam fluence, F, is fitted fairly well by:

$$S(F) = S_0 e^{-\sigma_d^{ap} F} - (S_0 - S_p) e^{-(\sigma_c + \sigma_d^{ap})F}, \quad (1)$$

The first term describes the two processes responsible for the disappearance of water molecules from the sample: destruction by water radiolysis and removal by sputtering; de Barros et al. (2012) described these two processes by $dS/dF = -\sigma_d^{ap} S$, where σ_d^{ap} is the apparent destruction cross section defined by the sum: $\sigma_d^{ap} = \sigma_d + Y_0/N_0$; σ_d quantifies the chemical destruction; Y_0/N_0 is the sputtering ice factor where Y_0 is the number of desorbed molecules per projectile and N_0 the initial column density. The second term of Eq. (1) describes the irradiation-induced compaction with the same expression Strazzulla et al. (1992) used for amorphization of crystalline water ice (CW), and also Leto and Baratta (2003) used to explain the transformation of p-ASW into ASW after irradiation. They used an exponential function $1 - exp(-\sigma_c F)$ to quantify the fraction of amorphization and compaction processes in the irradiated water ice. In the case of compaction of p-ASW samples, $S_0 > S_p$ occurs and a fast increase of the OH-stretch band area is seen at the beginning of irradiation (Fig. 2a). For CW samples, $S_0 < S_p$ occurs and a fast decrease in Eq. (1) is observed, a behavior also reported by Leto and Baratta (2003) (see Fig. 8 of their paper). We suggest that the ice compaction can be associated to the change from the initial band area of virgin porous ice, S_p, to the expected band area at $F = 0, S_0$, corresponding to the initial area of a virgin compacted ice. Therefore, the dependence of band area on fluence is:

$$S_c(F) = (S_0 - S_p) e^{-\sigma_c F}, \quad (2)$$

Eq. (2) describes the fast component of the band area variation, as depicted in Fig. 2; the cross section σ_c obtained in the current work is very close to the value found by Dartois et al. (2013) for the description of the OH-db collapse (see Table 1). Since the peak shift also evolves exponentially with the same decay parameter σ_c, this

Table 1
Summary of compaction data: ice mixture, ion beam and its energy, thickness, electronic stopping power S_e, and compaction cross section σ_c.

Ice	Position (cm^{-1})	Mixture	Thickness (μm)	Ion	Energy (MeV)	[g]S_e (10^{-15} eV cm^2/molec)	σ_c (10^{-13} cm^2)	Reference
H_2O:CO	3636	10:1	0.25	H^+	0.2	21.6	3.0	[a]
H_2O:CO_2	3657	10:1	0.25	H^+	0.2	22.1	2.5	[a]
H_2O:CH_4	3684, 3670	1:1	0.25	He^+	0.2	18.0	3.0	[a]
H_2O:CO_2	3657	5:1	0.25	He^+	0.2	56.2	3.4	[a]
H_2O:CO_2	3657	1:1	0.25	He^+	0.2	70.8	4.6	[a]
H_2O	3720, 3692	pure	0.44	Ar^+	0.1	53.3	1.5	[b]
H_2O:NH_3:CO	3650	10:6:4	1.7	Ni^{13+}	46	1538	100	[c]
H_2O	3720, 3692	pure	0.64	Zn^{26+}	606	974	80	[d]
H_2O	3720, 3692	pure	1.1	Ni^{11+}	46	1469	160	[d]
H_2O:NH_3	3692	10:1	1.8	Ni^{24+}	536	857	100	[e]
H_2O:H_2CO:CH_3OH	3720, 3692	100:2:0.8	0.33	O^{7+}	220	71.6	3.0	[f]
H_2O:CO_2	3657	1:1	0.6	Ni^{13+}	52	2048	72	This work
H_2O:CO_2	3657	10:1	0.5	Ni^{13+}	52	1576	32	This work
H_2O:CO	3636	1:1	~1	Ni^{13+}	52	1906	120	This work
H_2O:CH_4	3684, 3670	2:1	~1	Ni^{11+}	40	1300	71	This work
H_2O:CH_4	3684, 3670	10:1	~0.6	Ni^{11+}	40	1402	120	This work

[a] Palumbo (2006).
[b] Raut et al. (2007).
[c] Pilling et al. (2010).
[d] Dartois et al. (2013).
[e] Bordalo et al. (2013).
[f] de Barros et al. (2014).
[g] The electronic stopping power S_e was calculated using the SRIM program (Ziegler et al., 2010).

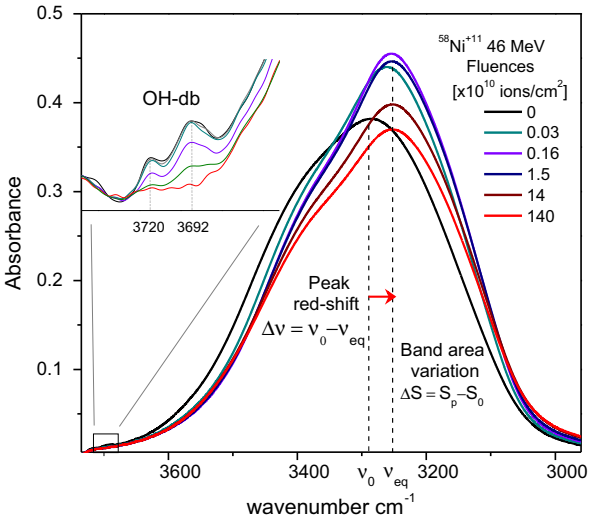

Fig. 1. IR spectra of porous amorphous water solid (p-AWS) at 15 K after and before 46 MeV Ni irradiation at several fluences (Dartois et al., 2013). The inset shows the decrease of the db-OH features, The OH-stretch band position is gradually red-shifted during irradiation from $\nu_0 = 3290\ cm^{-1}$ to $\nu_1 = 3250\ cm^{-1}$; the band area change as well. (For interpretation of the references to color in this figure legend, the reader is referred to the web version of this article.)

behavior is most likely another manifestation of the compaction process.

3.2. Spectral changes for pure p-ASW

As presented in Fig. 1, three spectral changes were observed during irradiation of pure H_2O at p-ASW: (i) the increase of the band area 3250 cm^{-1}; (ii) the shift of its peak position; and (iii) the collapse of OH-db features.

Fig. 2 shows the evolution of the integrated absorption of the 3250 cm^{-1} band and its position as a function of the fluence. Fig. 2a presents the band areas fitted by Eq. (1), while Fig. 2b shows that the shift of the band peak is approximately described by an exponential function plus a constant. For both cases presented in Fig. 2, the obtained cross sections (Ni or Zn) are approximately equal within the error bar (<5%). Fig. 3 shows the OH-db absorption, OH-stretch mode and peak position, all of them normalized at the beginning of irradiation, as a function of the ion dose $D = S_e \times F$, for 606 MeV Zn and 46 MeV Ni ion projectiles. Here S_e is the electronic stopping power (10^{-15} eV cm^2/molec) (Ziegler et al., 2010) and F is the beam fluence (ions/cm^2). The relevant point is that the variations follow an exponential decrease $exp(-D/D_0)$, where D_0 is approximately equal to 0.2 eV/molec for both beams, in agreement with Dartois et al. (2013).

3.3. Porous ices of H_2O:X mixtures

OH-db profiles of H_2O:X ice mixtures have been studied by many researchers. One important finding is that the peak positions of the dangling bonds depend on the interacting of species X with H_2O, in Table 1 are given these peaks positions (for the others H_2O:X ice mixtures see Palumbo et al. (2010)). The normalized areas of OH-db bands of the ices irradiated with swift heavy ions listed in Table 1 are depicted in Fig. 4. The box region of this figure corresponds to irradiations for which the OH-db integrated band area decreased to a value less than 10% of the initial one after 1 eV/molec of absorbed dose. The compaction cross sections (σ_c) are from previous publications. Palumbo (2006) used the light ions H and He to irradiate H_2O:X mixtures. Heavy ions were used by Raut et al. (2007) to irradiate pure water with 100 keV Ar^+. Other ices were studied by Pilling et al. (2010), Dartois et al. (2013), Bordalo et al. (2013) and de Barros et al. (2014).

Fig. 5a shows the band shift during the compaction processes for pure and mixed water ices. This behavior of pure water was pointed out by Leto and Baratta (2003) in their study on crystalline ice amorphization induced by UV photons. The exponential decrease corresponding to each shift for each sample has the same behavior that those found for the OH-db band area collapse shown in Fig. 4 and whose σ_c are listed in Table 1. In Fig. 5, the region delimited by the dashed box presented between 3250 and 3270 cm^{-1} ices corresponds to the compaction occurring under the deposited energy density of 1 eV/molec (this energy is clearly seen in Fig. 4). In the right side, corner of Fig. 5a, the three points represent the wavenumbers corresponding of water peak band after irradiation reported by Baratta et al. (1991), Leto and Baratta (2003) and Pilling et al. (2010). Additionally, astronomical

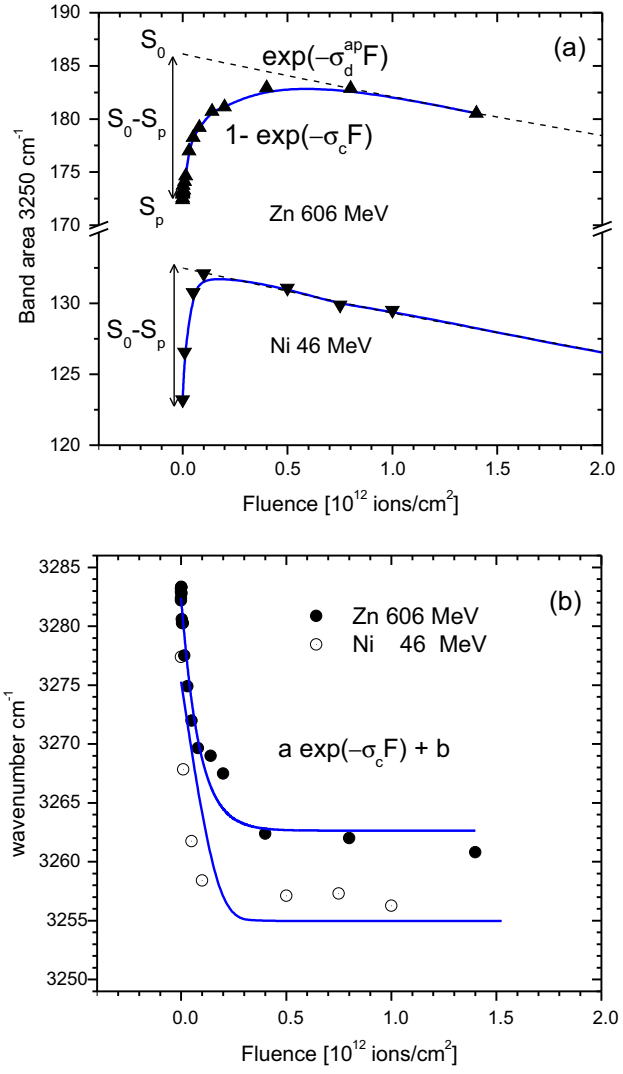

Fig. 2. (a) 3250 cm^{-1} band area evolution when amorphous H_2O at 15 K under heavy ion is irradiated by 606 MeV Zn and by 46 MeV Ni (top); the solid lines are fittings of data using Eq. (1) to obtain σ_c; (b) The shift of the 3250 cm^{-1} band position as a function of fluence. In both experiments the peak has shifted to lower wavenumbers (redshift); the solid lines are fittings using $y = a \cdot exp(-\sigma_c F) + b$, with a and b being arbitrary constants.

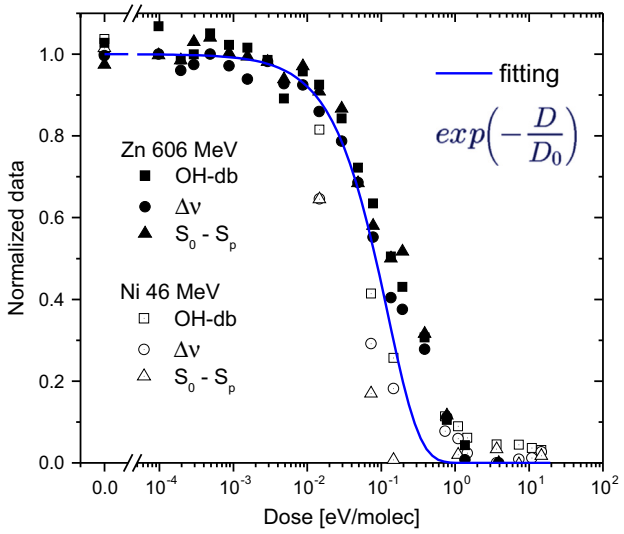

Fig. 3. Normalized data as a function of the doses $D = S_e \times F$, with $D_0 = S_e/\sigma_c$. Squares are OH-db peak areas, circles and triangles are peak shifts and band areas of OH-stretch mode, respectively. Note that these data have approximately the same exponential constant D_0 during compaction process.

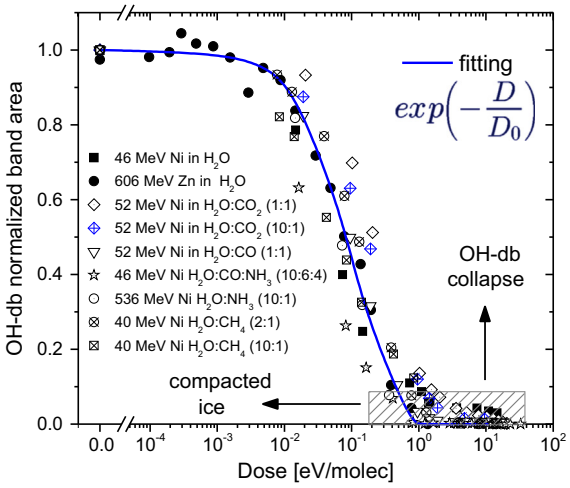

Fig. 4. OH-db absorbance decrease during irradiation. The hatched box indicates the region of the OH-db collapse when the compacted ice receives the energy density of 1 eV/molec from the projectile. The solid line corresponds to the exponential fitting of all data with $D_0 = 0.17 \pm 0.02$ eV/molec.

peak position values of OH-stretch mode, extracted from fitting of the figures of Baratta et al. (1991), Boogert et al. (2011) and Dartois et al. (2013), are presented in Fig. 5b. This comparison provides evidence from astronomical observations that astrophysical ices largely exposed to cosmic radiation are likely ASW compacted with minimal OH-db features.

In Table 1, the compaction cross sections obtained in the current analysis are compared with values reported for other projectile-ice systems. Fig. 6 depicts the same data as a function of the electronic stopping power S_e. As a conclusion, the relation $\sigma_c = S_e/D_0$ is approximately valid for pure and mixed ices containing water (more than 50% of H_2O), where D_0 lies between 0.08 and 0.5 eV/molec which takes the average value of 0.2 eV/molec.

4. Discussion

4.1. OH stretch area increase in p-ASW

Under irradiation, the OH-stretch mode band area of the p-ASW ice has been reported to increase up to 10% of its initial value by Leto and Baratta (2003) and Gomis et al. (2004). These authors concluded that this increase is due to the variation of the *A*-value ($\mathcal{A}_\nu$) induced by ion irradiation. Such an apparent increase of the number of molecules in the irradiated ice has caused a confusion in choosing correctly the initial column density (Pilling et al., 2010). In the current data, a 10% increase is also observed for the band area, indicating that $\mathcal{A}_\nu$ must be 10% higher than the value of 2×10^{-16} cm/molec found by Allamandola et al. (1988) for water ice film obtained at 10 K. This corresponds to the initial value of $\mathcal{A}_\nu(0) = 2 \times 10^{-16}$ cm/molec for p-ASW. We conclude that the quantity $\mathcal{A}_\nu$ varies during the compaction process and depends on dose D as:

$$\mathcal{A}_\nu(D) = \mathcal{A}_\nu^{eq}\left(1 - \zeta \cdot e^{-D/D_0}\right) \quad (3)$$

where $\mathcal{A}_\nu^{eq}$ is the *A*-value for the equilibrium ice state, obtained when $F \to \infty$. The quantity $\mathcal{A}_\nu^{p} = \mathcal{A}_\nu^{eq}(1-\zeta)$ is the *A*-value for the virgin porous ice, as usually reported in literature. ζ is a parameter

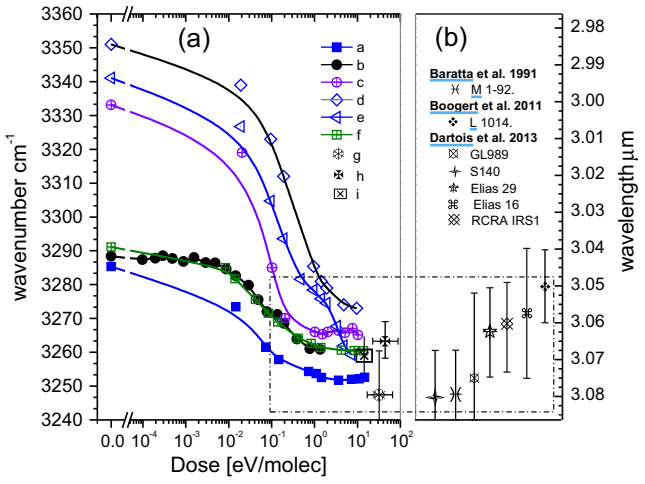

Fig. 5. (a) 3250 cm^{-1} band shift during compaction processes for the ices listed in Table 1: (a) Ni in pure H_2O, (b) Zn in pure H_2O, and mixtures: (c) H_2O:CO_2 (1:1), (d) H_2O:CO_2 (10:1), (e) H_2O:CO (1:1), (f) H_2O:CH_4 (10:1); additionally, the final band positions of water ices after laboratory irradiation of previous works are shown: (g) Baratta et al. (1991), (h) Leto and Baratta (2003), and (i) Pilling et al. (2010). (b) The astronomical peak positions (without a specific x axis) are displayed: Baratta et al. (1991), Boogert et al. (2011) and Dartois et al. (2013). In the box region, the band positions corresponding to compacted ice are indicated.

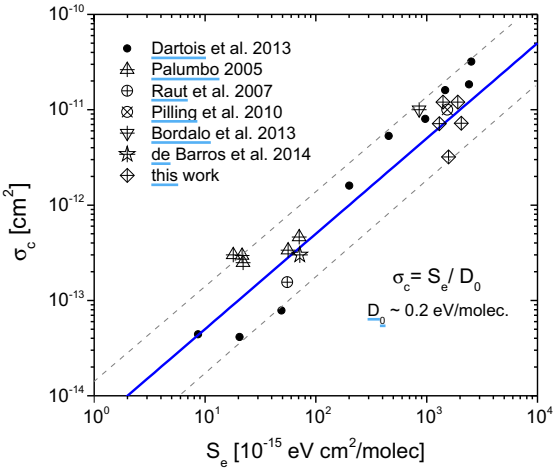

Fig. 6. Compaction cross section as a function of the electronic stopping power for pure and mixed water ices (see Table 1). Data correspond to water ice mixtures analyzed in the current work and include the results obtained by: Palumbo (2006), Raut et al. (2007), Pilling et al. (2010), Bordalo et al. (2013), Dartois et al. (2013) and de Barros et al. (2014). The solid line is found by fitting of $\sigma_c = S_e/D_0$ (with D_0 = 0.2 eV/molec), and the dotted lines show the boundaries of D_0 (at 0.08 and 0.5 eV/molec).

characterizing the porosity fraction of the virgin ice, or more generally, the relative initial abundance of different phases states. This connects the phenomenological description treated in Section 3.1 (Eq. (1)) with band strength A-values (IR absorption). The function $\mathcal{A}_v(F)$ given by Eq. (3) can now be introduced in the Lambert–Beer law to obtain the correct column density for p-ASW. This law is expressed by:

$$N(F) = ln10 \cdot \frac{S(F)}{\mathcal{A}_v(F)} \tag{4}$$

in which $S(F)$ represent the peak area of an IR transition. Note that $S(F)$ may vary during the compaction process but $N(F)$ should not. The column density at $F = 0$ writes $N(0) = ln10 \cdot S_p/\mathcal{A}_v(0)$ molec/cm^2. For p-ASW:

$$S(F) = S_0 e^{-\sigma_d^{ap} F} - S_0 \zeta e^{-(\sigma_c + \sigma_d^{ap})F}, \tag{5}$$

which is Eq. (1) if $\zeta = (S_0 - S_p)/S_0 = (\mathcal{A}_v^{eq} - \mathcal{A}_v^{p})/\mathcal{A}_v^{eq}$. For the current data, $\mathcal{A}_v^{eq} = 2.2 \times 10^{-16}$ cm/molec and $D_0 \sim 0.2$ eV/molec. The ζ value depends on the H_2O:X mixture and for pure water ice is equal to 0.1. This result is supported by the result of Bossa et al. (2012): they found a 12% ($\zeta = 0.12$) decrease of water ice thickness during a thermal process. Leto and Baratta (2003) reported around 15% for UV irradiation while Raut et al. (2008) determined 26% based on density changes of porosity (which was measured by specular light reflectance spectra). In the mixture H_2O:CO_2 (2:1), Isokoski et al. (2014) measured a reduction of 12% of porosity during thermal annealing.

4.2. Ion tracks in p-ASW

The interaction of energetic charged particles with surfaces has been described by Bethe (1932) and Bloch (1933) equation, where the electronic stopping power is analytically determined by:

$$S_e = \frac{4\pi Z_B (Z_A e^2)^2}{m_e v^2}\left[ln\left(\frac{2m_e v}{\bar{I}}\right) - \frac{C}{Z_B} - 1\right] \tag{6}$$

Z_A and Z_B are the atomic number of the target nucleus and projectile ion, respectively; m_e and e are the mass and charge of the electron, v is the ion velocity, $\bar{I}$ is the average ionization potential, and C is a factor associated with the shell structure of the target atom or molecule.

Inokuti (1971) estimated the ionization cross section σ_i for high velocities as:

$$\sigma_i \approx \frac{2m_e \bar{r}^2}{3\hbar^2} S_e \tag{7}$$

where $\bar{r}$ is the mean squared radius of the initial state. Comparing this equation with $\sigma_c = S_e/D_0$, obtained with data presented in Fig. 6, it follows that

$$\varepsilon_i = D_0 = \frac{3\hbar^2}{2m_e \bar{r}^2} \tag{8}$$

The parameter ε_i is the effective density of deposited energy by the ion required to compact p-ASW. Finally, from Eq. (8), considering $\varepsilon_i = D_0 = 0.2$ eV/molec, $\bar{r} \sim 8$ Å is obtained. The cylinder radius of around 10 Å was interpreted by Raut et al. (2008) as the maximum transverse range of the secondary electrons released by penetrating ions with hundreds keV of kinetic energy. The same value was attributed by Parent et al. (2002) to be the average size of pores diameter in porous water ice at 38 K using X-ray absorption fine structure technique.

In the literature, the absorption of energy by irradiated water have been intensively studied. Particular findings are: (i) the minimal photo absorbed energy of water ice is ~8 eV, as proposed by Mason et al. (2006); (ii) the threshold electron energy to destroy H_2O in solid phase and to produce H_2O_2 was found to be ~5 eV by Pan et al. (2004); (iii) the threshold energy for dissociation in gas phase of ~4.7 eV was estimated by Gudipati and Cooper (2013); and (iv) an effective density of deposited energy of 1.3 eV/molec to reduce the volume of p-ASW using ions with energies lower than 400 keV was obtained by Raut et al. (2008). Fig. 6 shows that the average deposited dose by ion beam is around 0.2 eV/molec. This value is less than those mentioned before and is related with the rearrangement of molecules (Dartois et al., 2013).

The linear dependence given by Eq. (7) has been attributed by Raut et al. (2008) to two physical effects in the ion track: (a) δ-electrons are released in the track after molecule ionization (Ritchie and Claussen, 1982), and (b) a thermal-spike process would be

responsible to the increase of the temperature along the track (Szenes, 1997). The first effect requires the ionization of water molecule of ions with energies above of ionization energy to generate δ-electrons, while the second effect neglects the nuclear collision for low energy ion beams ($v_B < 0.22$ cm/ns).

The formalism proposed by Toulemonde et al. (2011) has been successful in describing the structural modifications of vitreous SiO_2 using a thermal spike model that considers the synergy between the elastic (S_n) with inelastic (S_e) thermal spike model. This model could explain the scatter data observed in Fig. 6. In the current work, Eq. (7) is used to describe roughly the compaction processes for ices irradiated with high ion energies where the nuclear energy loss is negligible. Therefore, the deviation between model and experiment by a factor of $\leq$2.5 (from $D_0 = 0.2^{+0.3}_{-0.12}$ eV/molec) is within the range of acceptance suggested by Klaumuenzer (2006), as seen in Fig. 6.

4.3. Astrophysical consequences

4.3.1. Comparison with observations

The morphology of water ice in space depends on the astrophysical conditions of the ISM region. Observations indicate the presence of amorphous water ices (Boogert et al., 2011) in the quiescent molecular clouds, where the temperatures are about 10 K, In the circumstellar envelopes of evolved stars, where temperatures can exceed 100 K, observations indicate the presence of crystalline ices. Specifically, Baratta et al. (1991) demonstrated that the observed 3.1 μm band of the evolved star OH 231.8 + 4.2 can be approximated by the laboratory band of a crystalline ice condensed at 140 K, cooled at 77 K and irradiated by 3 keV He ions. Furthermore, Dartois et al. (2002) detected the amorphous and crystalline phase of ice mantles surrounding GL 989 and GL 2136.

At 10 K, water vapor condenses into an ASW. The ice porosity depends on the initial conditions of the experiment such as deposition rate, incident angle of the vapor jet, temperature and substrate. See Baragiola (2003) for a detailed discussion of water phases and microporosity. The absence of the OH-db signature in the observed IR spectra of ISM suggests that the ASW dust mantles, with sizes <2 μm (Kim et al., 1994), are non-porous or that the pores have collapsed by thermal or irradiation process in time scales lower that the molecular cloud lifetimes (Dartois et al., 2013 and references therein). Non-porous ASW can also be formed by surface reactions on dust grains which would explain the lack of OH-db band observation. However, given the great diversity of astrophysical environments, p-ASW may exist in the coldest regions.

Many laboratory experiments have demonstrated that both ice phases evolve to a common morphology under irradiation (Baragiola, 2003; Leto and Baratta, 2003; Palumbo, 2006; Dartois et al., 2013). If the ice is initially crystalline, the band shape broadens and shifts to lower frequencies, similar to the characteristic shape of an amorphous compact ice. If the ice is initially amorphous containing pores, the band becomes shaper and shifts to higher frequencies. However, regardless of the initial phase of the ice (amorphous or crystalline), the peak frequency of the OH-stretch band shifts to a wavenumber around 3260 cm^{-1} (Leto and Baratta, 2003). In the present work, similar behavior is demonstrated for pure and mixed amorphous ices, irradiated by heavy ions. Fig. 5 shows the peak frequency shift as a function of the heavy ion dose for all the ices studied here. The peak frequencies have moved to wavenumbers around 3260 cm^{-1}. This "intermediate" phase is related to an amorphous compacted ice Baragiola (2003), Palumbo (2006), Dartois et al. (2013). Palumbo (2006) showed that CO diffusion is prevented after an initially condensed p-ASW was subjected to keV–MeV H and He irradiation. This was interpreted as the collapse of the pores after ion irradiation. Dartois et al. (2013) studied the pores collapse induced by heavy ions by measuring the decrease of the OH-db at 2.7 μm.

The decrease of this band area induced by H and He ion irradiation for ice mixtures was previously reported by Palumbo (2006), and for heavy ion irradiation by Pilling et al. (2010). In the current work, the decrease of the OH-db area is also related to the peak shift of the OH-stretch band (Fig. 7). It shows a correlation between the decrease of OH-db with the peak shift of OH-stretch towards to the 3260 cm^{-1} wavenumber.

As shown by Fig. 5, there are a few examples of hot and dense cores in the ISM where water ice can present some level of porosity: L 1014, Elias 29 and Elias 16. The OH-stretch peaks of those objects have wavenumbers higher than 3260 cm^{-1}. Guided by the correlation shown in Fig. 7, the ice mantles present in those environments may have some porosity. This tentative relation between porosity and the OH-stretch peak needs to be considered with caution. There are many parameters that affect the observed 3 μm band position. They are: (i) the presence of crystalline ices in the line of sight, (ii) the presence of other molecules in the ice and (iii) the composition and geometry of the substrate (in the ISM the substrates are composed of dust grains with a complex morphology). New experiments need to be performed in order to confirm the correlation observed in Fig. 7. However, once confirmed, the astronomers will have another diagnostic tool to probe the morphology of water ice based on the band peak of OH-stretch, which is the main signature of water ice in ISM.

4.3.2. Compaction by solar wind

In previous work Dartois et al. (2013) calculated the compaction rates for ices irradiated by galactic cosmic rays (GCR). The half life ($\tau_{1/2}$) found is in the range from 10^5 to 2×10^6 years. The same procedure is used to estimated the half-life of OH-db, for ices observed in the outer Solar System. The estimations are based on the solar wind (SW) distribution of each ion Φ_i reported by Mewaldt et al. (2001) and Cohen et al. (2005). The integral of $\Phi_i \times \sigma_{c,i}$ (with $\sigma_{c,i}$ for the ion i) is the compaction rate to each ion, and the sum of all elements of SW is given by the total compaction rate $\mathcal{R}_{SW} = \Sigma \mathcal{R}_i$ (Mejía et al., 2013). In Table 2 some examples are presented. The compaction rate $\mathcal{R}_{SW}$ for H, He, C, O, S, Fe

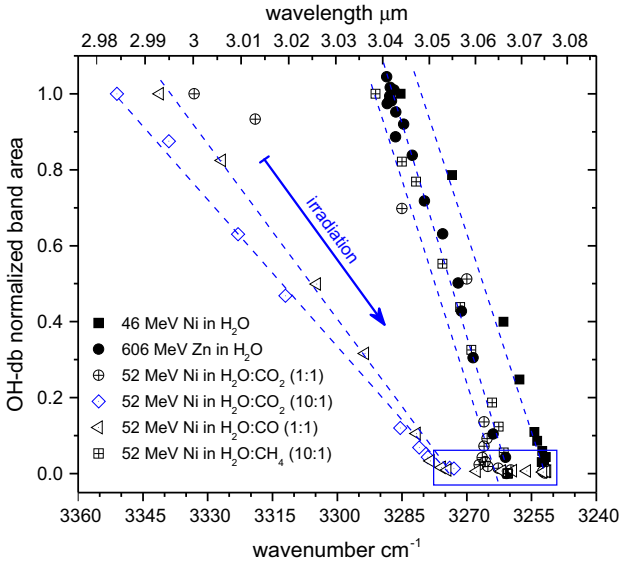

Fig. 7. Decrease of OH-db band area versus peak shift OH-stretch band during ion beam irradiation (in the arrow direction) of some ices of Table 1. In the box region is showed the minimal OH-db band area and the final OH-stretch band positions. The dashed lines are guides for the eyes.

Table 2
Compaction rates, $\mathcal{R}_j = \int \sigma_{cj} \times \Phi_j dE_n d\Omega$ for H_2O:X ices bombarded by H, He, O, C, S, Fe and Ni ions at the distance of 5.2 AU from the Sun.

Ion	$\mathcal{R}_j$ (s^{-1})
H	1.7×10^{-5}
He	2.3×10^{-6}
C	6.3×10^{-8}
O	1.2×10^{-7}
S	5.5×10^{-9}
Fe	4.7×10^{-9}
Ni	1.6×10^{-10}
$\mathcal{R}_{SW} = \Sigma \mathcal{R}_j$	2.0×10^{-5}

and Ni projectile ion is calculated for ices irradiated at a distance of 5.2 AU from the Sun; the half life of OH-db at this distance is about 9.6 h. The half life of OH-db to more external ices is $\tau_{1/2} = 260/D_\odot^2$ hr with $D_\odot$ the distance (in AU) from the Sun to the ice irradiated by the solar wind. Note that $\tau_{1/2}$ depends also on variations of solar activity, photon irradiation (Palumbo et al., 2010), magnetosphere of some solar bodies and its temperature.

5. Conclusions

Irradiation of solid samples may cause sputtering (removal of material), chemical reactions (destruction and formation of molecular species) and structural modifications (compaction, amorphization, crystallization). Concerning the structural changes, there are evidences that MeV ion irradiation of ices takes the sample into an equilibrium state in which the ice is well compacted but having a stable mixture of amorphous and crystalline fractions.

In this work, pure water ices and H_2O:X (X = CO, CO_2 and CH_4) mixture have been bombarded by heavy fast ions. The produced effects were analyzed by infrared spectroscopy. The main findings are:

- The compaction process in water ice can be monitored by three quantities: OH-stretch mode band area increase, OH-stretch mode peak position shift and areas of the OH-db peaks collapse. The evolution of these quantities as a function of the beam dose is analyzed.
- During the compaction process, the band area increases and the peak position of OH-stretch mode shows a linear correlation with OH-db peak area.
- The compaction of mixtures H_2O:X (X = CO, CO_2, NH_3, CH_4, CH_3OH and H_2CO; where H_2O is >50%) and pure water follow a similar dependence with dose.
- The IR absorption A-value, $\mathcal{A}_v$, depends on dose, D, as $\mathcal{A}_v(D) = \mathcal{A}_v^{eq}\left(1 - \zeta \cdot e^{-D/D_0}\right)$. D_0 is the mean dose value for the compaction process. The parameter ζ is defined as $\zeta = (\mathcal{A}_v^{eq} - \mathcal{A}_v^{p})/\mathcal{A}_v^{eq}$ gives the fraction of the porous ice phase before irradiation. A typical value is $\zeta \sim 0.1$. A more general interpretation of the same parameter is that it quantifies the relative absorbance variation observed for the initial deposited ice, $\mathcal{A}_v(0)$, and in the limit of highest dose, $\mathcal{A}_v^{eq}$.
- Porous ice mixtures H_2O:X, exposed to GCR, become compact within of 1×10^5 to 2×10^6 years in the ISM (in agreement with previous calculations). For ices inside the Solar System, the compaction process depends on the distance from the Sun to the ice, following the law $\tau_{1/2} = 260/D_\odot^2$ hr (with $D_\odot$ in AU).
- For high fluences, the peak position of the OH-stretch band ranges from 3270 to 3245 cm^{-1} (or wavelengths from 3.05 to 3.08 μm). This behavior is consistent with astronomical observations.

Acknowledgments

This work was supported by the French-Brazilian exchange program CAPES-COFECUB. The Brazilian agencies CNPq (INEspaço) and FAPERJ are also acknowledged. We thank J.J. Ding, T. Langlinay, T. Been, C. Grygiel, T. Madi, I. Monnet and J.M. Ramillon for their invaluable support.

References

Accolla, M. et al., 2013. Morphology of the solid water synthesized through the pathway D + O_2 studied by the sensitive TPD technique. Mon. Not. R. Astron. Soc. 429 (4), 3200–3206.
Allamandola, L.J., Sandford, S.A., Valero, G.J., 1988. Photochemical and thermal evolution of interstellar/precometary ice analogs. Icarus 76 (2), 225–252.
Baragiola, Raúl A., 2003. Water ice on outer Solar System surfaces: Basic properties and radiation effects. Planet. Space Sci. 51 (14), 953–961.
Baragiola, R.A., Fama, M., Loeffler, M.J., Raut, U., Shi, J., 2008. Radiation effects in ice: New results. Nucl. Instrum. Methods Phys. Res., Sect. B 266 (12), 3057–3062.
Baragiola, R.A. et al., 2013. In The Science of Solar System Ices. Springer, New York, pp. 527–549.
Baratta, G., Leto, G., Spinella, F., Strazzulla, G., Foti, G., 1991. The 3.1 micrometers feature in ion-irradiated water ice. Astron. Astrophys. 252, 421–424.
Baratta, G.A., Brunetto, R., Leto, G., Palumbo, M.E., Spinella, F., Strazzulla, G., 2004. Ion irradiation of ices relevant to astrophysics. Memorie della Soc. Astronom. Ital. Supplementi 5, 33–36.
Bethe, Hans, 1932. Brake formula for relativistic electron velocity. J. Phys. 76 (5–6), 293–299.
Bloch, Felix, 1933. Bremsvermögen von Atomen mit mehreren Elektronen. Zeitschrift fr Physik A Hadrons Nuclei 81 (5), 363–376.
Boogert, A.C.A. et al., 2011. Ice and dust in the quiescent medium of isolated dense cores. Astrophys. J. 729 (2), 92–108.
Bordalo, V. et al., 2013. Chemical processing of pure ammonia and ammonia-water ices induced by heavy ions. Astrophys. J. 774 (2), 105–118.
Bossa, J.B., Isokoski, K., de Valois, M.S., Linnartz, H., 2012. Thermal collapse of porous interstellar ice. Astron. Astrophy. A82, 545–550.
Brown, W.L., Lanzerotti, L.J., Poate, J.M., Augustyniak, W.M., 1978. Sputtering of ice by MeV light ions. Phys. Rev. Lett. 40 (15), 1027–1030.
Cheung, A.C., Rank, D.M., Townes, C.H., Thornton, D.D., Welch, W.J., 1969. Delection of water in interstellar regions by its microwave radiation. Nature 221, 626–628.
Collado, V.M., Farenzena, L.S., Ponciano, C.R., Da Silveira, E.F., Wien, K., 2004. Ion desorption from frozen H_2O irradiated by MeV heavy ions. Surface Sci. 569 (1), 149–162.
Cohen, C. et al., 2005. Heavy ion abundances and spectra from the large solar energetic particle events of October–November 2003. J. Geophys. Res.: Space Phys. 110 (A9), 1978–2012.
Dartois, E., 2005. The Ice Survey Opportunity of ISO. ISO Science Legacy. Springer, pp. 293–310.
Dartois, E., d'Hendecourt, L., Thi, W., Pontoppidan, K.M., Van Dishoeck, E.F., 2002. Combined VLT ISAAC/ISO SWS spectroscopy of two protostellar sources. The importance of minor solid state features. Astron. Astrophys. 394, 1057–1068.
Dartois, E. et al., 2013. Swift heavy ion irradiation of water ice from MeV to GeV energies. Approaching true cosmic ray compaction. Astron. Astrophys. 557, 97–105.
de Barros, A.L.F., Farenzena, L.S., Andrade, D.P.P., da Silveira, E.F., Wien, K., 2011. Secondary ion emission from water ice at 10–130 K induced by MeV N_2^+ ions. J. Phys. Chem. C 115 (24), 12005–12014.
de Barros, A.L.F., Boduch, P., Domaracka, A., Rothard, H., da Silveira, E.F., 2012. Radiolysis of astrophysical ices by heavy ion irradiation: Destruction cross section measurement. Low Temp. Phys. 38 (8), 759–765.
de Barros, A.L.F., da Silveira, E.F., Pilling, S., Domaracka, A., Rothard, H., Boduch, P., 2014. Processing of low carbon content interstellar ice analogues by cosmic rays: Implications for the chemistry around oxygen-rich stars. Mon. Not. R. Astron. Soc. 438 (3), 2026–2035.
Gibb, E.L., Whittet, D.C.B., Boogert, A.C.A., Tielens, A.G.G.M., 2004. Interstellar ice: The infrared space observatory legacy. Astrophys. J. Suppl. Ser. 151 (1), 35–73.
Gillett, F.C., Forrest, W.J., 1973. Spectra of the Becklin–Neugebauer point source and the Kleinmann–Low nebula from 2.8 to 13.5 microns. Astrophys. J. 179, 483–491.
Gomis, O., Satorre, M.A., Strazzulla, G., Leto, G., 2004. Hydrogen peroxide formation by ion implantation in water ice and its relevance to the Galilean satellites. Planet. Space Sci. 52 (5), 371–378.
Gudipati, Murthy S., Cooper, Paul D., 2013. Chemistry in water ices: From fundamentals to planetary applications. In: The Science of Solar System Ices. Springer, New York, pp. 503–526.
Inokuti, Mitio, 1971. Inelastic collisions of fast charged particles with atoms and molecules: The Bethe theory revisited. Rev. Modern Phys. 43 (3), 297–347.
Isokoski, Karoliina, Bossa, J-B., Triemstra, Thomas, Linnartz, H., 2014. Porosity and thermal collapse measurements of H_2O, CH_3OH, CO_2, and H_2O:CO_2 ices. PCCP 16 (8), 3456–3465.

Johnson, R.E., 2011. Photolysis and radiolysis of water ice. In: Khriachtchev, L. (Ed.), Chapter 10 in Physics and Chemistry at Low Temperatures. World Scientific, Singapore, pp. 297–339 (Published by Pan Stanford Publishing Pte. Ltd).
Kim, Sang-Hee, Martin, P.G., Hendry, Paul D., 1994. The size distribution of interstellar dust particles as determined from extinction. Astrophys. J. 422, 164–175.
Klaumuenzer, S., 2006. Thermal-spike models for ion track physics: A critical examination. In: Sigmund, P. (Ed.), Ion Beam Science: Solved and Unsolved Problems, Pts 1 and 2. Royal Acad. Sci. & Letters, pp. 293–328.
Lanzerotti, L.J., Brown, W.L., Poate, J.M., Augustyniak, W.M., 1978. On the contribution of water products from Galilean satellites to the jovian magnetosphere. Geophys. Res. Lett. 5 (2), 155–158.
Leto, G., Baratta, G.A., 2003. Ly-α photon induced amorphization of Ice water ice at 16 Kelvin effects and quantitative comparison with ion irradiation. Astron. Astrophys. 397, 7–13.
Mason, Nigel J. et al., 2006. VUV spectroscopy and photo processing of astrochemical ices: An experimental study. Faraday Discuss. 133, 311–329.
Mejía, C. et al., 2013. Cosmic ray–ice interaction studied by radiolysis of 15 K methane ice with MeV O, Fe and Zn ions. Mon. Not. R. Astron. Soc. 433, 2368–2379.
Mewaldt, R., et al., 2001. Long-term fluences of energetic particles in the heliosphere. In: International Cosmic Ray Conference, vol. 10, pp. 3984–3987.
Moore, M.H., Hudson, R.L., 2000. IR detection of H_2O_2 at 80 K in ion-irradiated laboratory ices relevant to Europa. Icarus 145 (1), 282–288.
Mumma, Michael J., Charnley, Steven B., 2011. The chemical composition of comets Emerging taxonomies and natal heritage. Astron. Astrophys. 49 (1), 471–524.
Oba, Y., Miyauchi, N., Hidaka, H., Chigai, T., Watanabe, N., Kouchi, A., 2009. Formation of compact amorphous H_2O ice by codeposition of hydrogen atoms with oxygen molecules on grain surfaces. Astrophys. J. 701 (1), 464–470.
Palumbo, M.E., 2006. Formation of compact solid water after ion irradiation at 15 K. Astron. Astrophy. 453 (3), 903–909.
Palumbo, M.E., Baratta, G.A., Leto, G., Strazzulla, G., 2010. H bonds in astrophysical ices. J. Mol. Struct. 972 (1), 64–67.
Pan, X., Bass, A.D., Jay-Gerin, J.P., Sanche, L., 2004. A mechanism for the production of hydrogen peroxide and the hydroperoxyl radical on icy satellites by low-energy electrons. Icarus 172 (2), 521–525.
Parent, Ph., Laffon, C., Mangeney, C., Bournel, F., Tronc, M., 2002. Structure of the water ice surface studied by X-ray absorption spectroscopy at the OK-edge. J. Chem. Phys. 117 (23), 10842–10851.
Pilling, S. et al., 2010. Radiolysis of ammonia-containing ices by energetic, heavy and highly charged ions inside dense astrophysical environments. Astron. Astrophys. A87, 509–519.
Pontoppidan, K.M., van Dishoeck, E.F., Dartois, E., 2004. Mapping ices in protostellar environments on 1000 AU scales: Methanol-rich ice in the envelope of Serpens SMM 4. Astron. Astrophys. 426 (3), 925–940.
Ponciano, C.R., Farenzena, L.S., Collado, V.M., da Silveira, E.F., Wien, K., 2005. Secondary ion emission from CO_2–H_2O ice irradiated by energetic heavy ions: Part II: Analysis search for organic ions. Int. J. Mass Spectrom. 244 (1), 41–49.
Raut, U., Teolis, B.D., Loeffler, M.J., Vidal, R.A., Fama, M., Baragiola, R.A., 2007. Compaction of microporous amorphous solid water by ion irradiation. J. Chem. Phys. 126 (24), 244511–244516.
Raut, U., Famá, M., Loeffler, M.J., Baragiola, R.A., 2008. Cosmic ray compaction of porous interstellar ices. Astrophys. J. 687 (2), 1070–1074.
Ritchie, R.H., Claussen, Carsten, 1982. A core plasma model of charged particle track formation in insulators. Nucl. Instrum. Methods Phys. Res. 198 (1), 133–138.
Rowland, Brad, Paul Devlin, J., 1991. Spectra of dangling OH groups at ice cluster surfaces and within pores of amorphous ice. J. Chem. Phys. 94 (1), 812–813.
Seperuelo Duarte, E. et al., 2009. Heavy ion irradiation of condensed CO_2: Sputtering and molecule formation. Astron. Astrophys. 502, 599–603.
Smith, Bradford A. et al., 1989. Voyager 2 at Neptune: Imaging science results. Science 246 (4936), 1422–1449.
Strazzulla, G., Baratta, G.A., Leto, G., Foti, G., 1992. Ion-beam induced amorphization of crystalline water ice. EPL (Europhys. Lett.) 18 (6), 517–522.
Strazzulla, Giovanni, Palumbo, Maria Elisabetta, 1998. Evolution of icy surfaces: An experimental approach. Planetary Space Sci. 46 (9), 1339–1348.
Szenes, G., 1997. Amorphous track formation in SiO_2. Nucl. Instrum. Methods Phys. Res., Sect. B 122 (3), 530–533.
Toulemonde, Marcel et al., 2011. Synergy of nuclear and electronic energy losses in ion-irradiation processes: The case of vitreous silicon dioxide. Phys. Rev. B 83 (5), 054106, p. 9.
Whittet, D.C.B., 2003, . Dust in the Galactic Environment, second ed., vol. 1. Institute of Physics Publishing, Bristol.
Yabushita, Akihiro, Hama, Tetsuya, Kawasaki, Masahiro, 2013. Photochemical reaction processes during vacuum-ultraviolet irradiation of water ice. J. Photochem. Photobiol., C 16, 46–61.
Ziegler, James F., Ziegler, M.D., Biersack, J.P., 2010. SRIM The stopping and range of ions in matter (2010). Nucl. Instrum. Methods Phys. Res., Sect. B 268 (11), 1818–1823.